Megadroughts in the Indian Monsoon Region and Southwest North America and a Mechanism for Associated Multidecadal Pacific Sea Surface Temperature Anomalies

GERALD A. MEEHL AND AIXUE HU

National Center for Atmospheric Research,* Boulder, Colorado

ABSTRACT

A 1360-yr control run from a global coupled climate model (the Parallel Climate Model) is analyzed. It simulates "megadroughts" in the southwestern United States and Indian monsoon regions. The megadroughts represent extreme events of naturally occurring multidecadal precipitation variations linked to the dominant pattern of multidecadal SST variability in the Indian and Pacific Oceans. Gaining insight into the occurrence of megadroughts thus requires an understanding of the mechanism that is producing this multidecadal SST variability. Analysis of the model variability shows that the mechanism involves atmosphere–ocean and tropical–midlatitude interactions, with a crucial element being wind-forced ocean Rossby waves near 20°N and 25°S in the Pacific whose transit times set the decadal time scale. At the western boundary, the Rossby waves reflect into the equatorial Pacific to affect thermocline depth. The resulting feedbacks, involving surface temperature, winds, and the strength of the subtropical cells, produce SST anomalies and associated precipitation and convective heating anomalies. These anomalies are associated with atmospheric Rossby waves and resulting anomalous atmospheric circulation patterns in the midlatitude North and South Pacific. Consequent surface wind stress anomalies extend equatorward into the Tropics and help force ocean Rossby waves near 20°N and 25°S, and so on. Though there are some common elements with various ENSO processes, this decadal mechanism is physically distinct mainly because the surface wind stress anomalies near 20°N and 25°S supplement the wave reflections at the eastern boundary to force the ocean Rossby waves that provide the decadal time scale. These wind anomalies are closely tied to the anomalous midlatitude atmospheric circulation that is a product of teleconnections from the multidecadal SST and tropical convective heating anomalies, themselves linked to precipitation anomalies in the southwestern United States and south Asia associated with megadroughts.

---

1. Introduction

Droughts on the interannual time scale are a naturally occurring feature of the climate system, and, for North America, have been associated with sea surface temperature (SST) and convective heating anomalies in the tropical Pacific Ocean (Trenberth and Branstator 1992). Droughts associated with Indian monsoon failure, also occurring on the interannual time scale, are similarly well-documented characteristics of climate in the south Asian region and are associated with SST

anomalies in the tropical Pacific and Indian Oceans (Meehl 1987; Rasmusson and Carpenter 1983; Meehl and Arblaster 2002). Droughts on the decadal time scale (i.e., such as the 1930s drought in the United States or the recent North American drought that occurred over a roughly 5–10-yr time period) have severe impacts and have also been linked to SST anomalies in the tropical Pacific (Schubert et al. 2004; Hoerling and Kumar 2003). Similar decadal time scale droughts in the south Asian monsoon region have been connected to low-frequency SST variations in the tropical Pacific (Barlow et al. 2002; Krishnan and Sugi 2003). Even longer-lasting droughts, termed "megadroughts" and lasting for multiple decades, can have even more devastating impacts. Such a megadrought that occurred in the sixteenth century was associated with hemorrhagic fever epidemics that are believed to have killed up to 80% of the native population of Mexico (Acuna-Soto et al. 2002). A comparable long-lasting drought is thought

Corresponding author address: Dr. Gerald A. Meehl, National Center for Atmospheric Research, P.O. Box 3000, Boulder, CO 80307.
E-mail: meehl@ncar.ucar.edu

to have affected much of the western United States a few centuries prior to that (Cook et al. 2004).

Since there are indications that droughts on interannual and decadal time scales are linked to tropical Pacific SST anomalies, we hypothesize that megadroughts on the multidecadal time scale may also be associated with persistent SST anomalies on that time scale in that region. If this is the case, then tracing the cause of megadroughts lies with understanding the mechanism that produces multidecadal time-scale SST anomalies in the tropical Pacific. This multidecadal time scale has been identified to be associated with a distinct pattern of Pacific SSTs (Zhang et al. 1997), and mechanisms of decadal time-scale variability must invoke processes that can produce such a pattern on that time scale. Such mechanisms have been proposed based mainly on analyses of global coupled climate model simulations. These can be traced to coupled interactions over various regions of the Pacific, and invoke different dynamical mechanisms in the ocean and usually involve ocean–atmosphere coupling (e.g., Latif and Barnett 1994; Gu and Philander 1997; Kleeman et al. 1999; Knutson and Manabe 1998; Miller and Schneider 2000; Nonaka et al. 2002; Capotondi and Alexander 2001; Liu et al. 2002; Lee and Fukumori 2003; Liu and Yang 2003; Wu et al. 2003; Solomon et al. 2003; Jin 1997; Meehl et al. 1998; Schneider et al. 2002). Some of these involve some type of teleconnection between low and high latitudes through the atmosphere (e.g., Pierce et al. 2000; Liu et al. 2002; Deser et al. 2004).

The purpose of this paper is to identify megadroughts in a 1360-yr-long control simulation with a global coupled climate model, show that they are extremes of multidecadal precipitation anomalies associated with the previously documented multidecadal pattern of persistent SST anomalies in the Pacific, and trace the physical mechanism responsible for producing such long-lived anomalies of SSTs and associated megadroughts.

2. Model, observed data, and analysis framework

We use a fully coupled global climate model, the National Center for Atmospheric Research (NCAR)–Department of Energy Parallel Climate Model (PCM), that is described by Washington et al. (2000). The resolution of the atmosphere is T42, or roughly 2.8° × 2.8°, with 18 levels in the vertical. Resolution in the ocean is roughly ⅔° degree down to ½° degree in the equatorial Tropics, with 32 levels. There is a land surface model (Bonan 1996) and a dynamic and thermodynamic sea ice formulation. No flux adjustments are used in the model, and a stable surface climate is simulated. That is, for the 1360-yr-long control integration, there is only a

very small cooling trend of globally averaged surface air temperatures of roughly 0.03 K per century. The interannual climate variability related to ENSO is in reasonable agreement with observations (Meehl et al. 2001; Dai et al. 2001b). A 1500-yr-long control run has been completed with this model (with constant atmospheric constituents and radiative forcing) and, as noted above, we analyze the last 1360 yr of this simulation and focus on dynamical mechanisms in a particular 300-yr period. This period is considered to be representative of processes occurring in the rest of the simulation in that it contains megadroughts for both the southwestern United States and India. Special processing is performed for this period to transform the ocean history tape data to isopycnal surfaces to facilitate analysis of the multidecadal mechanism.

The PCM is a well-documented global coupled climate model that has been run for a large number of twentieth- and twenty-first-century climate simulations. The four-member ensemble simulations of twentieth-century climate with various combinations of observed forcings, including greenhouse gases, direct effect of sulfate aerosols, tropospheric and stratospheric ozone, solar, and volcanoes (Meehl et al. 2003, 2004a; Ammann et al. 2003), show good agreement with the time series of globally averaged surface air temperatures (Meehl et al. 2004a). Additionally, a number of future climate simulations have been performed with a business-as-usual scenario [Dai et al. 2001a; similar to the average of the Special Report on Emissions Scenarios (SRES)], a stabilization scenario (Dai et al. 2001a), and five different SRES scenarios: A2, A1B, B1 (Meehl et al. 2005), B2, and A1FI. This particular model is on the lower end of the climate sensitivity range in comparison with other models, with an equilibrium climate sensitivity to a doubling of CO_2 of 2.1°C, and a transient climate response (defined as the temperature change at the time of CO_2 doubling in a 1% yr^{-1} CO_2 increase experiment) of 1.3°C (Meehl et al. 2004b).

The observed SST dataset we use is a version produced by the Hadley Centre (Rayner et al. 2003), and the gridded land precipitation dataset is from New et al. (2001). The two regions we consider in this study with regard to megadroughts include the southwestern United States, termed the "Great Basin" (32°–42°N, 118°–106°W; note that the boundaries of this region extend over a larger area than the strictly defined Great Basin in Nevada), and the Indian monsoon region (5°–40°N, 60°–100°E).

There is no accepted standard definition of a megadrought. In fact, there are a multitude of different definitions of droughts in general (e.g., Glantz 1987, 1994), some based on precipitation deficits, some on sustained

soil moisture deficits, some on both, some taking into account evapotranspiration effects involved with vegetation or agriculture, some involving human influence on the land surface, and so on. Inherent in most of these definitions is some aspect of a precipitation deficit. Therefore, for a simple definition directly involving a sustained precipitation deficit that is consistent with the characteristics described in the introduction, we define a megadrought here based on a duration threshold as an 11-yr running mean of regional area-averaged precipitation anomalies less than zero for at least 20 consecutive years. We acknowledge that there could be many more ways to formulate such a definition, but as will be shown in the analyses to follow, the mechanisms and phenomena are dominant on the multidecadal time scale, so this simple concept is likely indicative of the coupled interactions on these multidecadal time scales involving sustained SST anomalies associated with long-lived precipitation anomalies.

3. Time scales of megadroughts in the model

To identify time scales of low-frequency variability associated with possible megadroughts in the model, we first show spectra of area-averaged annual mean precipitation time series from the 1360-yr control run for the two areas identified above. For the Great Basin (Fig. 1a), there are significant peaks at interannual time scales ranging from 2 to about 7 yr in association with the tropospheric biennial oscillation (TBO; Meehl 1997; Loschnigg et al. 2003) and ENSO in the model (Meehl et al. 2001). Both the TBO and ENSO have connections from the tropical Pacific SSTs to the Great Basin region, such that when the tropical Pacific SSTs are anomalously warm, there is greater-than-average precipitation in this region. There is a significant peak near 20 yr (see scale at top of panel) indicative of multidecadal precipitation variability in this region in the model.

With regard to the Indian monsoon region (Fig. 1b), there are similar significant peaks on the interannual time scales also connected with the TBO and ENSO, where positive SST anomalies in the tropical Pacific are associated with precipitation deficits in the Indian monsoon (e.g., Meehl and Arblaster 1998). For low-frequency variability, there is a significant peak near 30 yr, and one at about 140 yr (see scale at top of panel).

Thus, for both the Great Basin and Indian monsoon regions, there are statistically significant peaks at multidecadal (20–30 yr) time scales, suggesting that major droughts could occur at those time scales in the model.

To examine the low-frequency character of area-averaged precipitation for these regions, we first show the time series of 11-yr running annual mean precipi-
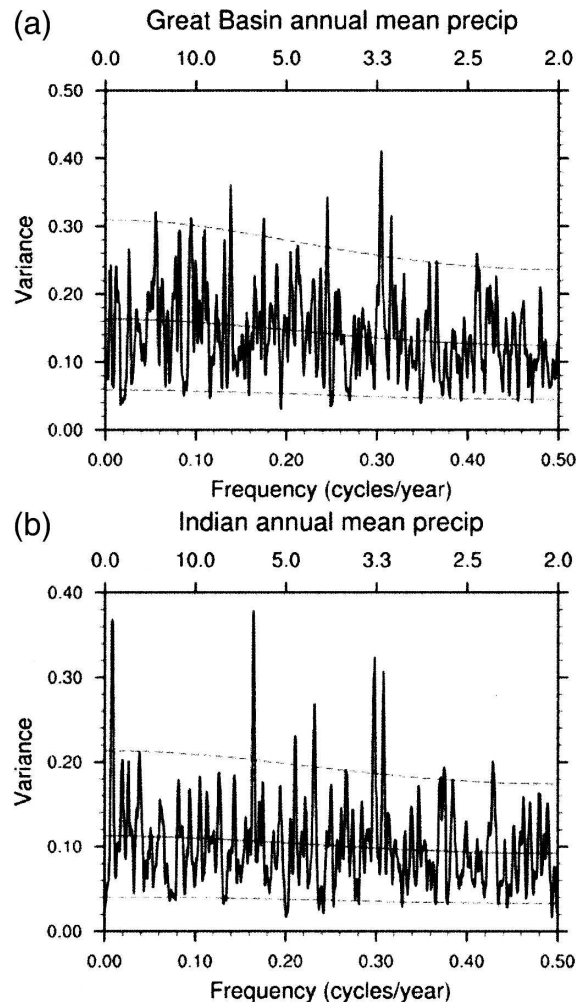

FIG. 1. Spectra of the annual mean precipitation for the (a) Great Basin region in the southwestern United States (as defined in the text) and (b) Indian monsoon region. The dashed line at the top is the 95% confidence level.

tation for the Great Basin area covering 1360 yr from the model control run simulation (Fig. 2). The low-frequency character suggested by the multidecadal spectral peak in Fig. 1 is clearly evident in this time series. If we apply the megadrought threshold definition given earlier, there are eight megadroughts in this time period, averaging one roughly every 170 yr. Thus, megadroughts meeting our threshold criteria are longer-lived extremes of naturally occurring multidecadal precipitation variability.

The concept of a megadrought implies relentless precipitation deficits over a multidecadal period. However, the reality of the model's manifestations of such a phenomenon indicates that during a megadrought, there are actually years when precipitation is near normal or even above normal. Figure 3 shows the annual mean
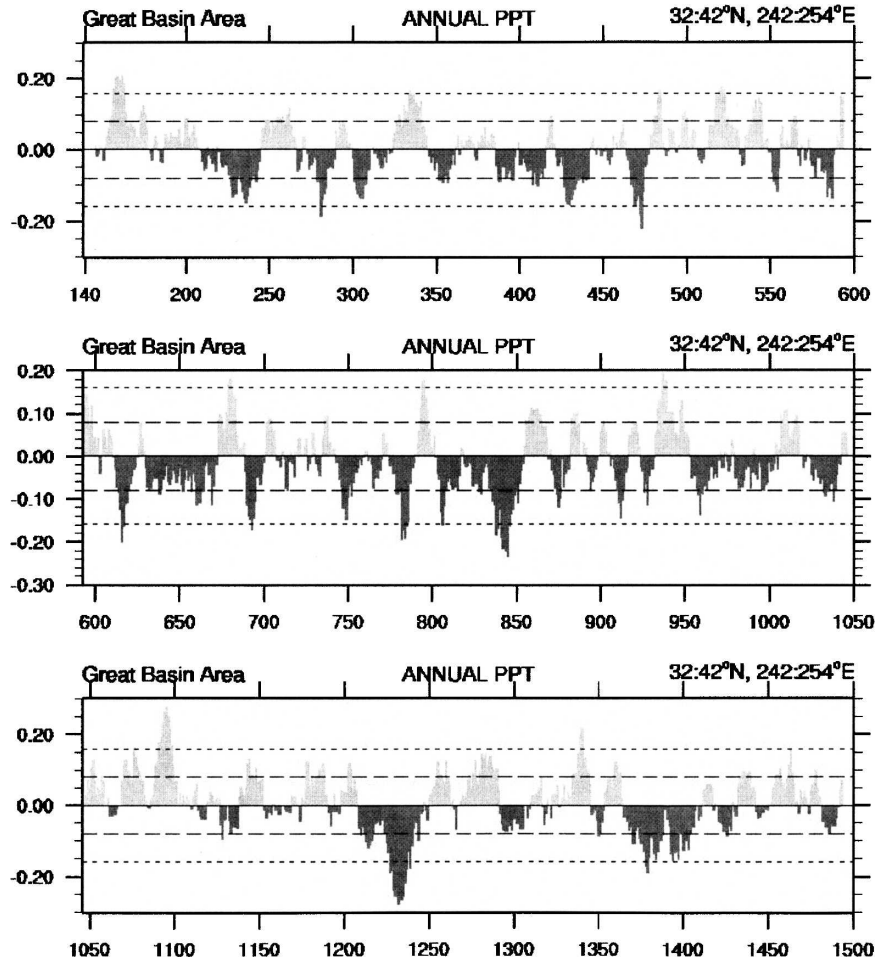
Fig. 2. Time series of the 11-yr running mean area-averaged annual precipitation (mm day^{-1}) for the Great Basin region in the southwestern United States for last 1360 yr of the 1500-yr PCM control simulation.

precipitation anomalies for one of the defined mega-droughts that occurred over the years 823–853 for the Great Basin region. Over that 31-yr period of the mega-drought, 20 yr have below-normal precipitation, while 11 yr have above-normal precipitation. Therefore, though we define this as a megadrought, about one-third of the years still have above-normal precipitation, indicating that a megadrought defined in this way indi-
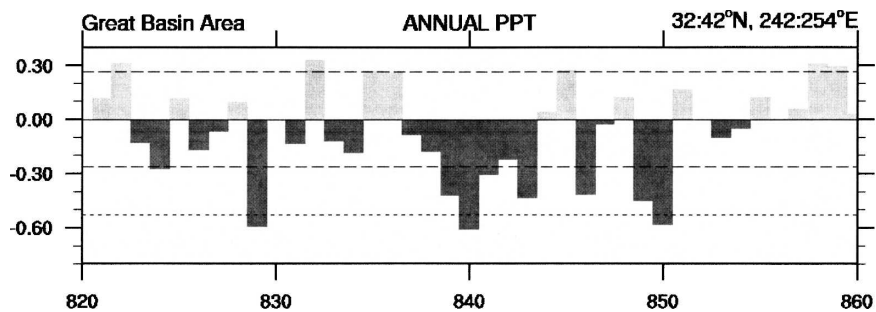

Fig. 3. Time series of the area-averaged annual mean precipitation with no filtering (mm day^{-1}) for one particular megadrought (as defined in the text) over the Great Basin region in the southwestern United States from the 1360-yr control run period (years 823–853).

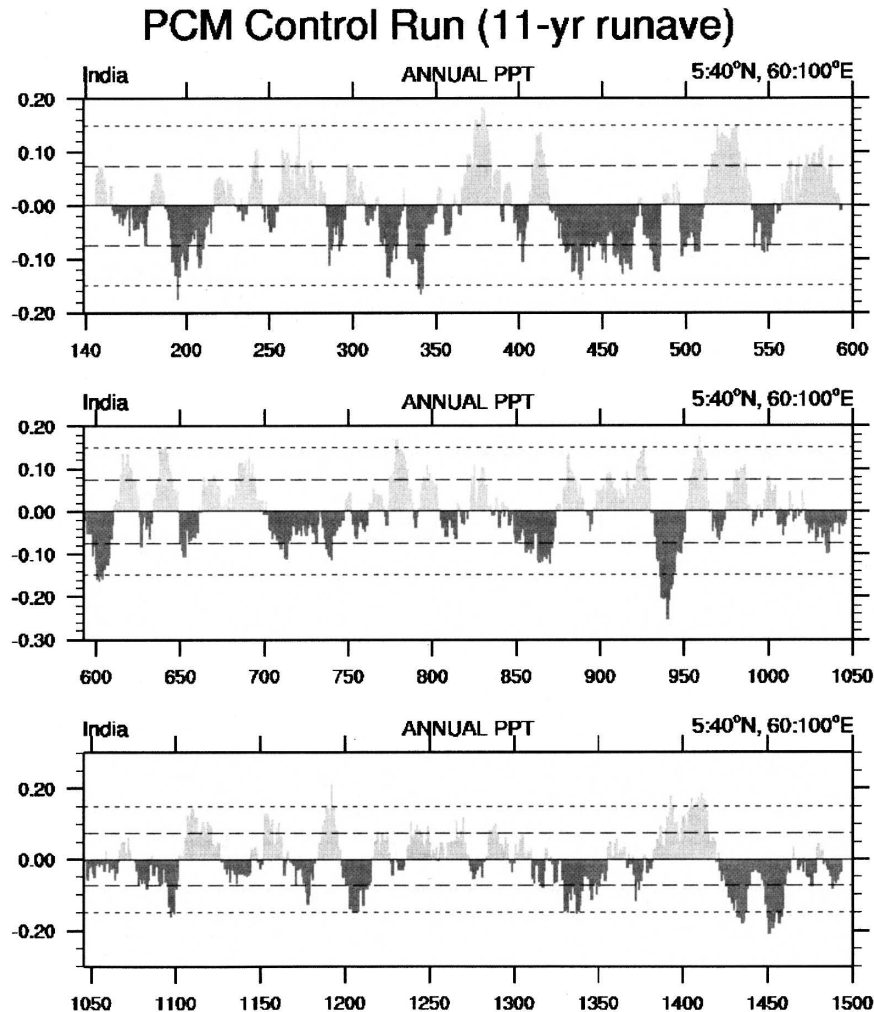## PCM Control Run (11-yr runave)

FIG. 4. Same as Fig. 2, but for the Indian monsoon region.

cates a shift in occurrence of precipitation anomalies toward proportionately more dry years than wet years over several decades.

The time series of 11-yr running annual mean precipitation anomalies for the Indian monsoon region is shown in Fig. 4. There are eight megadroughts in this 1360-yr time series, averaging one every 170 yr. As seen for the Great Basin region, these are also the longer-lived extremes of inherent multidecadal precipitation variability. To examine the interannual character of one of these megadroughts, Fig. 5 shows the annual mean time series for the megadrought that occurred in this region during the model years 851–875. During the 25-yr period of the megadrought, 18 yr had negative precipitation anomalies. Thus for both the Great Basin and Indian monsoon regions, a megadrought is characterized not by a continuous series of years with below-normal precipitation over several decades, but instead

by a shift of precipitation variability toward more precipitation-deficit years than precipitation-excess years over a multidecadal period. This suggests that impacts associated with megadroughts could be cumulative, with the majority of precipitation deficit years over a certain time period overwhelming the fewer number of years with positive precipitation anomalies. It is also evident from both the time series that megadroughts, arbitrarily defined based on a duration threshold, are the longer-lived manifestations of inherent multidecadal precipitation variability. Therefore, we must understand the mechanism that produces this multidecadal variability to gain insight into the megadrought phenomenon.

4. Long-lived SST anomalies and megadroughts

It was noted earlier that droughts over North America and in the Indian monsoon region on the in-
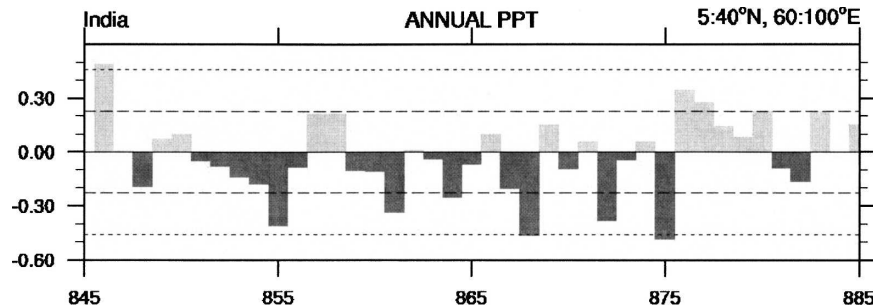
FIG. 5. Same as Fig. 3, but for an Indian monsoon region megadrought for the years 851–875.

terannual and decadal time scales tend to be associated with distinct SST anomaly patterns in the Pacific in models and observations. To identify the dominant SST anomaly patterns associated with multidecadal precipitation deficits in the model, we first low-pass filter the model annual mean SST data with a 13-yr cutoff to retain the multidecadal time scales and then correlate those low-pass-filtered SSTs with similarly low-pass-filtered time series of area-averaged annual mean Great Basin and Indian monsoon region precipitation for a 300-yr period (Fig. 6; other time periods show similar patterns and relationships). Taking into account autocorrelation effects in the filtered data (Leith 1973) and computing the actual degrees of freedom to be roughly 50 in this and the correlation plots to follow, correlation values greater in magnitude than about ±0.3 are significant at the 5% level.

Both regions show connections to the so-called "decadal" pattern of SST anomalies in the Pacific (e.g., Zhang et al. 1997), with same-sign values in a broad triangular-shaped area in the tropical Pacific, and opposite-sign values in the northwest and southwest Pacific. Correlations in the tropical Pacific in Fig. 6a are positive, indicating that multidecadal drought conditions in the Great Basin region are associated with negative SST anomalies over much of the tropical Pacific, similar to conditions associated with droughts over the southwestern United States on shorter time scales, as noted earlier.

For the Indian monsoon region in Fig. 6b, correlations over the tropical Pacific are negative, indicating that multidecadal time-scale drought conditions over the Indian monsoon region are associated with positive SST anomalies in the tropical Pacific. There are opposite-sign correlations in the northwest and southwest Pacific, also similar to conditions associated with monsoon deficits on shorter time scales noted above.

To investigate whether the model is simulating these relationships as observed, Fig. 7 shows a similar calculation to that in Fig. 6 but using the observations of gridded precipitation and SST data from 1901–2000. Area averages for the two regions are correlated to observed annual mean SSTs. Both observed datasets have been low-pass filtered with the same 13-yr cutoff as the model data in Fig. 6. For the Great Basin region, comparing Fig. 7a from the observations to Fig. 6a for the model, both show positive correlations in the tropical Pacific with opposite-sign correlations in the northwest and southwest Pacific. Similarly, for the Indian monsoon region, there are negative correlations in the
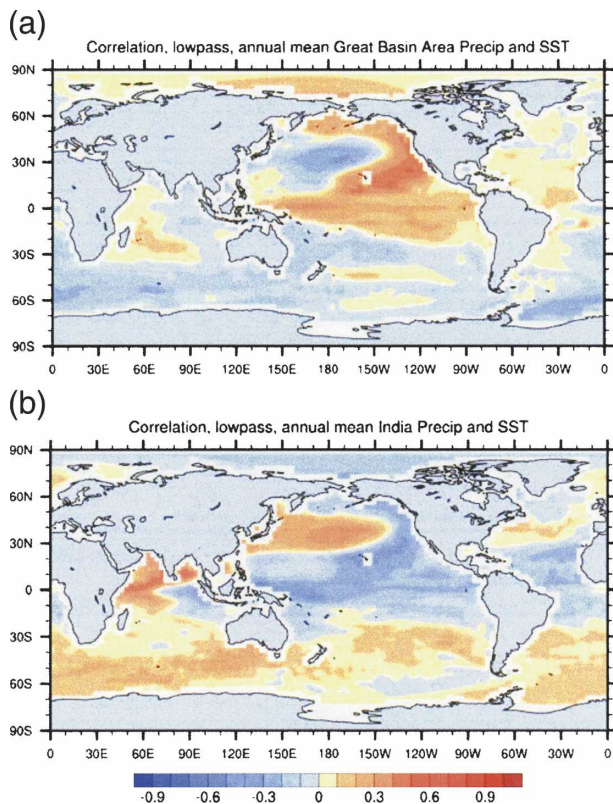

FIG. 6. Correlation of the 13-yr low-pass-filtered area-averaged precipitation for the (a) Great Basin area in the southwestern United States and (b) Indian monsoon region with similarly filtered SST at all other grid points for the 1360-yr control run.
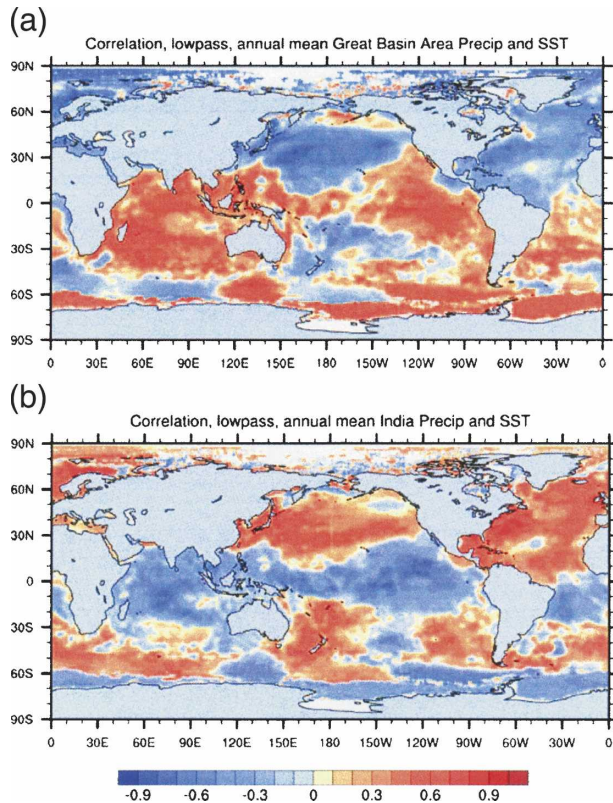
FIG. 7. Same as Fig. 6, but for observations from 1901 to 2000.

tropical Pacific with opposite-sign correlations to the northwest and southwest. The biggest difference in comparing the model correlation patterns in Fig. 6 to the observations in Fig. 7 is in the Indian Ocean. The observations show mostly same-sign correlations in the Indian and Pacific Oceans in Fig. 7, while the model has a mixture of signs of correlations in the Indian Ocean. This illustrates the influence of the Pacific on multidecadal droughts in the Indian monsoon region in the model and the observations, similar to that for the interannual time scales mentioned earlier.

To verify that the correlation patterns noted in Fig. 7 for observations are consistent with the dominant multidecadal pattern of SSTs, Fig. 8a shows the first EOF of low-pass-filtered observed SSTs (13-yr cutoff as in Fig. 7), which is very similar to the correlation pattern in Fig. 7, and resembles the decadal SST pattern of Zhang et al. (1997). Here we call this pattern the interdecadal Pacific oscillation (IPO) after Power et al. (1999) and Arblaster et al. (2002). This is a pattern that describes multidecadal time-scale variability over most of the Pacific Ocean, as compared with the Pacific decadal oscillation (PDO) that is defined for low-frequency SST variability in the North Pacific (Mantua et al. 1997). However, the PDO closely resembles as-

pects of the IPO in the North Pacific region, suggesting that similar mechanisms may be involved in both North Pacific and greater Pacific region multidecadal SST variability. In contrast, the interannual pattern in Fig. 8b shows greater magnitude values for EOF1 in the equatorial eastern Pacific, and opposite-sign anomalies in the western equatorial Pacific, also similar to the interannual pattern of SSTs in Zhang et al. (1997).

If we correlate the expansion coefficient time series from the IPO in Fig. 8a with low-pass-filtered gridded precipitation, the connections to the Great Basin region and the Indian monsoon region are evident in Fig. 9. There are mostly positive correlations over southwestern North America (indicating that precipitation deficits there are associated with negative SST anomalies in the tropical Pacific), and mostly negative correlations over the Indian monsoon region (indicating that precipitation deficits there are associated with positive SST anomalies in the tropical Pacific).

For the model, the low-pass-filtered EOF1 SST pattern is shown in Fig. 10a, with the interannual EOF1 pattern in Fig. 10b. Comparing the model multidecadal EOF SST pattern in Fig. 10a with the observed IPO in Fig. 8a, there are strong similarities in the Pacific, with the opposite-sign anomalies in the Indian Ocean being different from the observations (as seen in Fig. 6). For the interannual pattern in Fig. 10b, as shown before for this model and others, the ENSO variability in the tropical Pacific extends across to the western Pacific where in the observations there are opposite-sign values. Otherwise, there are larger values in the equatorial Pacific in Fig. 10b when compared with the off-equatorial maxima in the model IPO in Fig. 10a. We can check the spatial dependence of the IPO with precipitation and sea level pressure (SLP) in the model by correlating the expansion coefficient time series from the model IPO in Fig. 10a with low-pass-filtered precipitation and SLP in Fig. 11. Comparing Fig. 11a from the model to the comparable figure from the observations (Fig. 9), the connections to southwestern North America and the Indian monsoon are readily apparent, with positive correlations over most of western North America and negative correlations over the Indian monsoon region. This indicates that the model is capturing the essential elements of the multidecadal associations between tropical Pacific SSTs and precipitation over the Great Basin and Indian monsoon regions.

For SLP in Fig. 11b, an ENSO-like pattern is apparent with negative correlations over the eastern Pacific and North America, and positive correlations over south Asia. These results and those in the previous figures indicate that a similar set of global teleconnections to those on the interannual time scale are acting on the

(a)
Observed decadal pattern (1871-2000), "IPO", >13 yr low-pass

(b)
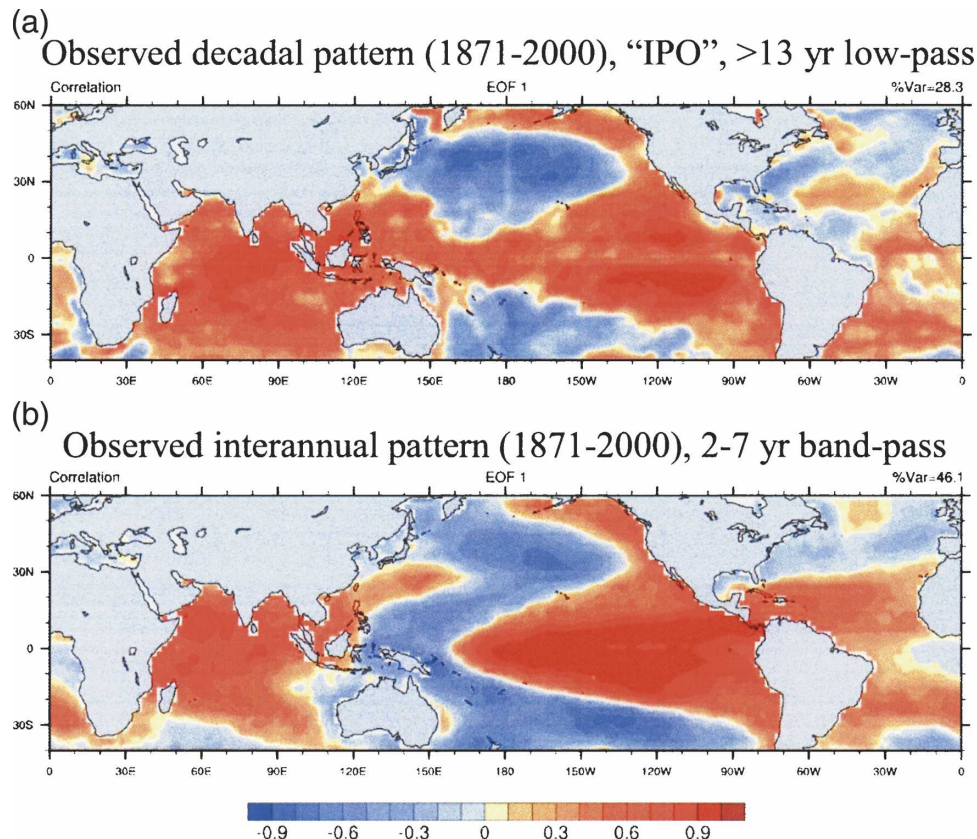## Observed interannual pattern (1871-2000), 2-7 yr band-pass

FIG. 8. The first EOF of (a) detrended 13-yr low-pass-filtered observed SSTs for the period 1871–2000 (referred to as the IPO in the text) and (b) 2–7-yr bandpass-filtered SST highlighting the interannual or ENSO pattern for the period 1871–2000.

multidecadal time scale. However, the mechanism that can produce and sustain such SST anomalies for the multidecadal time scale must be understood to be able to provide insight into the connections between long-lived droughts and Pacific SSTs.

One indication may be provided by the connections between the interannual and multidecadal time scales. As documented for this model by Arblaster et al. (2002), warm multidecadal periods in the tropical Pacific are associated with lower-amplitude El Niño variability when compared with cool IPO periods. Arblaster et al. (2002) showed that warm periods in the IPO in this model have a deeper equatorial eastern Pacific thermocline and consequently lower-amplitude El Niño events, and vice versa for cool IPO periods. This is consistent with the sensitivity experiments that showed that a deeper and more diffuse thermocline in the equatorial Pacific produces lower-amplitude El Niño events in this model (Meehl et al. 2001).

5. Multidecadal SST mechanism

It has been noted that the shallow subtropical cells (STCs) in the Pacific could be associated with multide-

cadal variability of SSTs in that region in observations (McPhaden and Zhang 2002) and in models (Kleeman et al. 1999; Nanoka et al. 2002; Solomon et al. 2003). The STCs in the PCM are shown in Fig. 12 as the zonally averaged meridional streamfunction plotted on isopycnal surfaces. An STC index is computed as the difference in the maximum value of the meridional overturning streamfunction, 9°N minus 9°S. This index is highly correlated with a similarly calculated heat transport index ($r = +0.75$) and is negatively correlated with the IPO index noted above ($r = -0.63$). That is, when heat transport out of the equatorial central Pacific is large, the STCs are strong, and SSTs are negative in the IPO. The latter is consistent with previous results (e.g., Kleeman et al. 1999).

Figure 13 shows the correlation of the STC index, as defined above, with SST, SLP, and precipitation. The correlation pattern of the multidecadal STC with SST in Fig. 13a closely resembles the IPO pattern in Fig. 10a, with a sign reversal. The correlation patterns of SLP and precipitation with the STC index (Figs. 13b,c) are also similar to the low-pass-filtered multidecadal correlation patterns with IPO in Figs. 11a,b. Therefore,
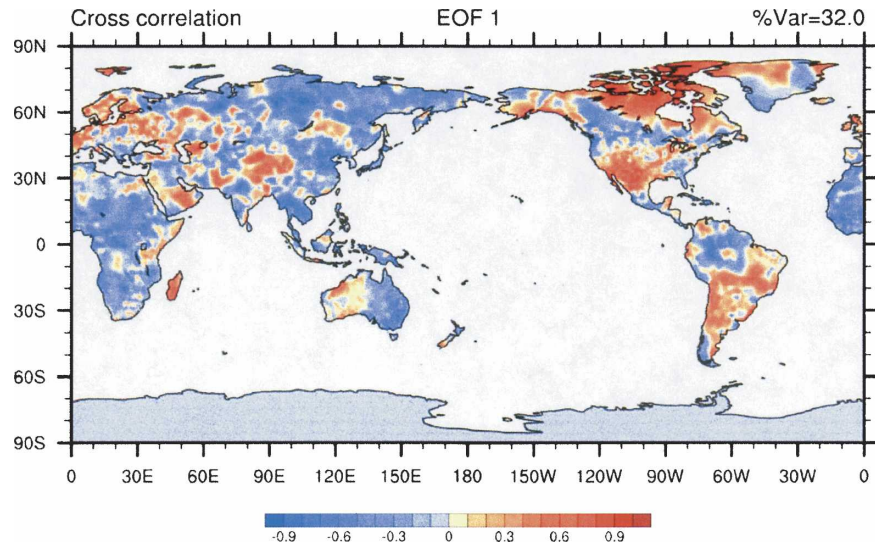
FIG. 9. Correlation of the principal component (PC) time series from the IPO in Fig. 8a
with 13-yr low-pass-filtered land precipitation for the period 1901–2000.

the STCs are connected to multidecadal tropical SST
variability.

The SLP correlations with the IPO in Fig. 11b indi-
cate that when tropical Pacific SSTs are warm, there are

deeper Aleutian and South Pacific low pressure centers
with associated stronger surface westerlies near 20°–
30°N and S, which is indeed the case if composites of
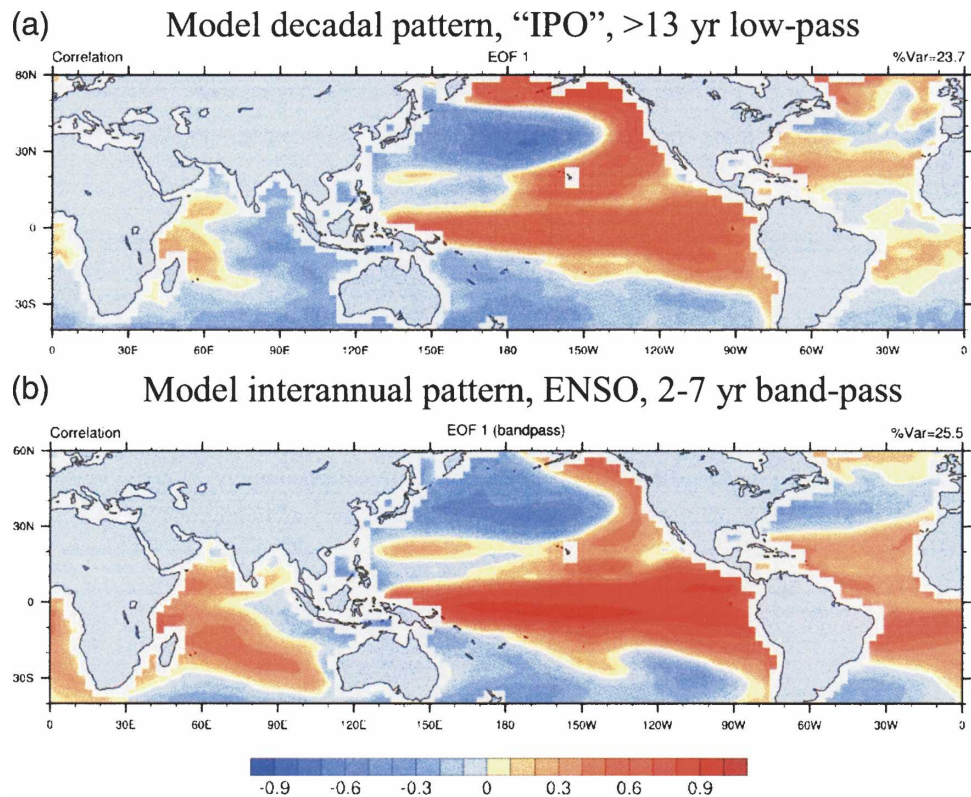warm IPO events are calculated (not shown). The role

FIG. 10. (a) Same as Fig. 8a, but for the model from the 1360-yr control run; (b) same as Fig. 8b, but
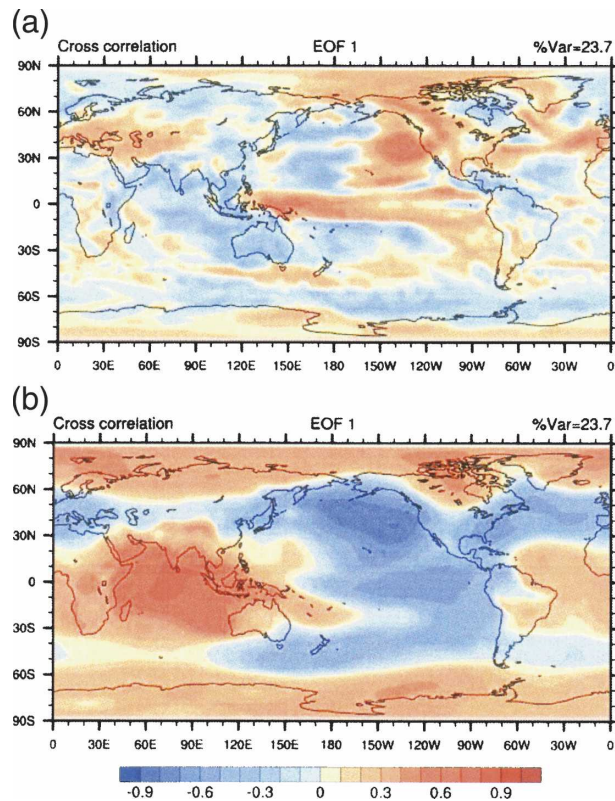from the model.

FIG. 11. Correlation of the PC time series from the model IPO in Fig. 10a with 13-yr low-pass-filtered model (a) precipitation and (b) SLP for the period 1901–2000.

of this remote SLP and associated surface wind response will prove to be critical as an atmospheric bridge (e.g., Alexander et al. 2002; Deser et al. 2004) to link multidecadal tropical Pacific SST anomalies with midlatitude circulation anomalies that act back on the
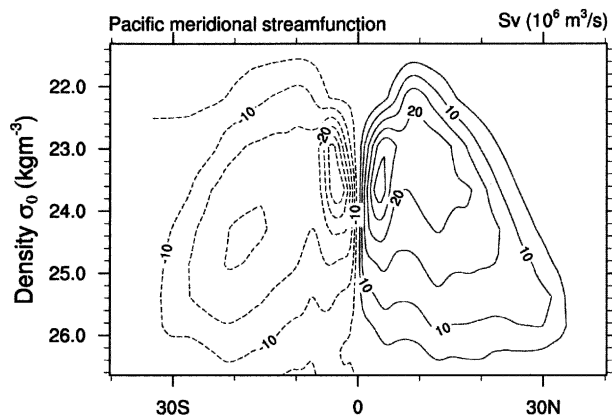

FIG. 12. Meridional overturning streamfunction (Sv; 1 Sv ≡ 10^6 m^3 s^{-1}) plotted on isopycnal surfaces for the Pacific basin from the model for the 1360-yr control run depicting the STCs.
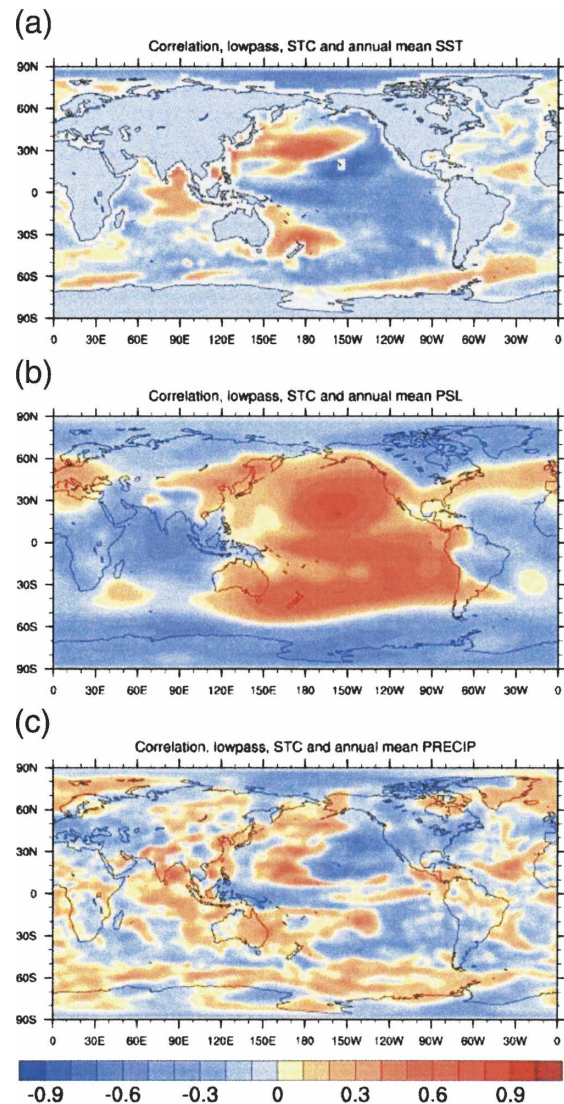

FIG. 13. Correlation of the low-pass-filtered STC index with similarly low-pass-filtered (13 yr) (a) SST, (b) SLP, and (c) precipitation from the 1360-yr model control run.

ocean to produce a turnabout of the tropical Pacific SST anomalies through dynamically coupled interactions.

To illustrate these connections, we take the 300-yr period from the control run, low-pass filter the data as before to retain the multidecadal time scales, and in Fig. 14 plot a Hovmöller diagram at 20°N (the latitude is chosen to be near the poleward extent of the northern STC in Fig. 12) zonal wind stress anomalies (right) with corresponding depth anomalies of the 26.6 sigma isopycnal surface (left). This surface is chosen based on the lower depth limit of the STCs in Fig. 12. At far right are plots of the IPO index and the STC index for this period, noting their opposite correlation as shown
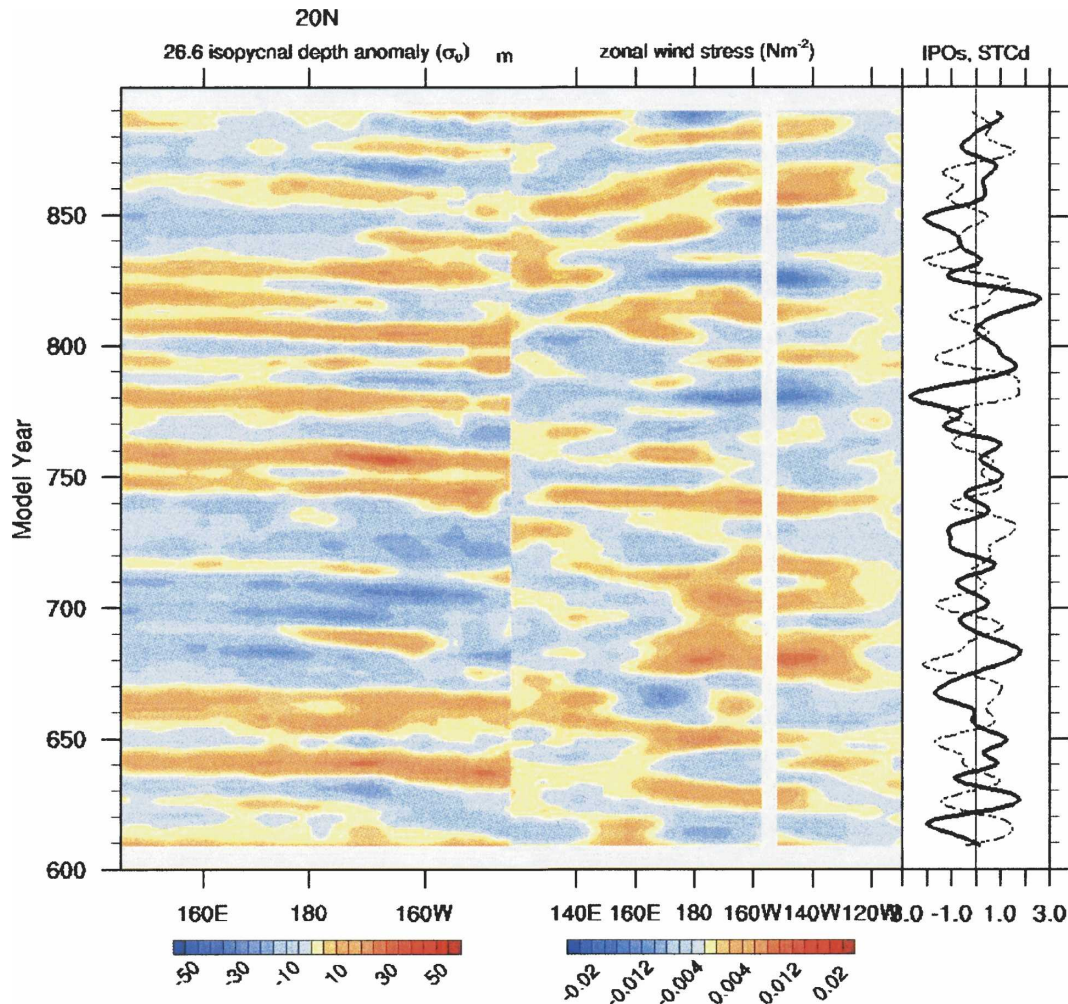
FIG. 14. (right) The low-pass-filtered IPC index (solid) and STC index (dashed). (middle) The Hovmöller diagram of low-pass-filtered wind stress anomalies (N m^{-2}) at 20°N from 120°E to 110°W from a 300-yr period in the control run for ocean points only (blank space is the Hawaiian islands). (left) Same as at right, but for depth anomalies of the 26.6 sigma isopycnal surface (m) from 140°E to 150°W at 20°N.

above (correlation is −0.47 for this time period). During periods of anomalous positive zonal wind stress (positive u component wind stress anomalies; wind stress curl anomalies that act to deepen the thermocline occur at comparable time periods) at 20°N, positive 26.6 sigma depth anomalies are generated in the eastern Pacific and propagate to the west at about 3 cm s^{-1}. Using a longwave approximation, the phase speed of a mode-1 Rossby wave at 20°N is about 3–5 cm s^{-1} (Gill 1982) and the time for this wave to cross the Pacific is roughly 9–13 yr.

Periods of positive zonal wind stress anomaly (at right) do not always generate Rossby waves (at left). For example, a large positive zonal wind stress anomaly near year 680 at right produces little in terms of a positive depth anomaly at left. But for other periods there

is a clear connection. For example, there are positive wind stress anomalies associated with positive depth anomalies (with positive IPO and negative STC at far right) near years 625, 650, 750, 820, and 850. There are negative wind stress anomalies with negative depth anomalies (and negative IPO and positive STC at far right) around years 615, 665, 720, 780, and 840. It is worth noting as well that the zonal wind stress values are plotted for ocean points only, thus the gap in wind stress data near 155°W at the right where the Hawaiian islands intervene.

Figure 15 is a comparable plot but for 25°S (near the poleward extent of the southern STC in Fig. 12) showing a similar relationship, with westerly anomaly wind stresses forcing positive 26.6 sigma depth anomalies that propagate westward at about 2 cm s^{-1}. At 25°S,
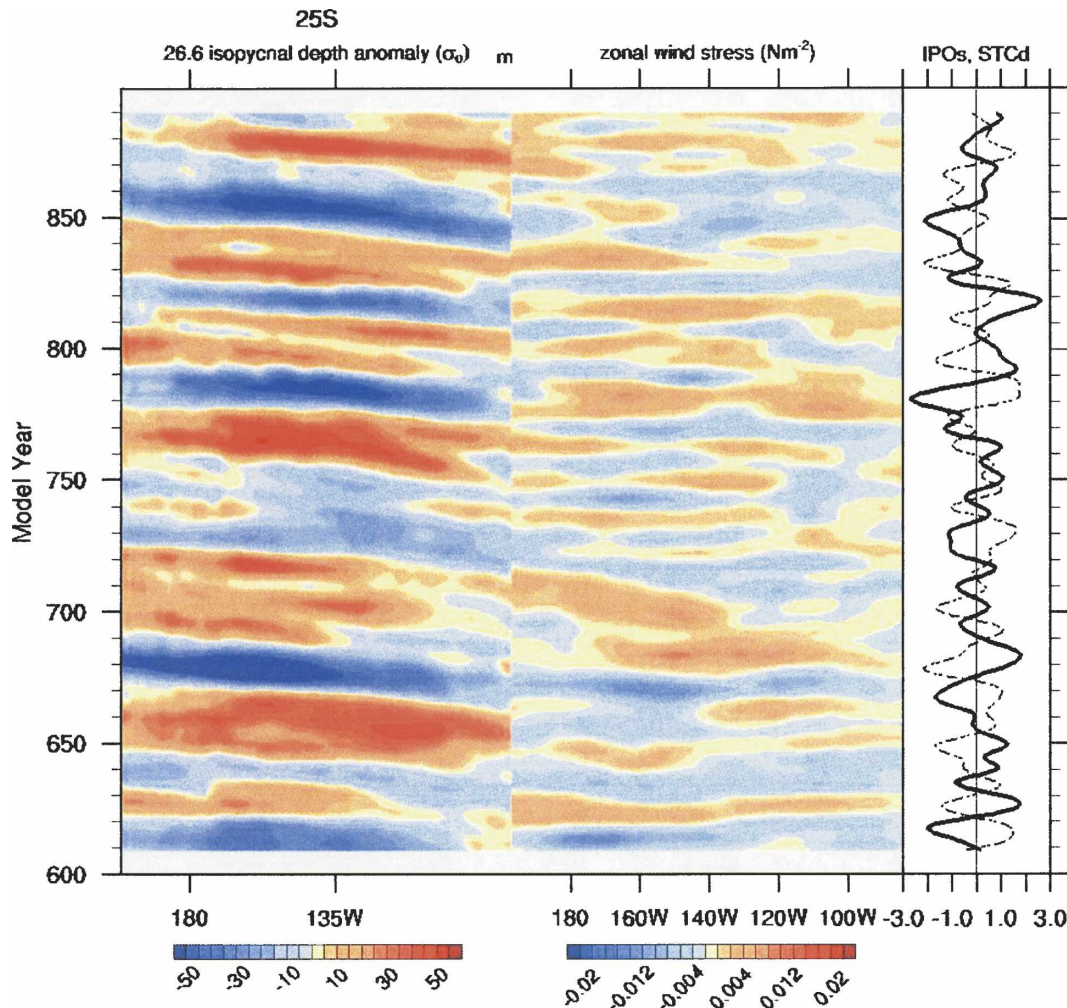
FIG. 15. Same as Fig. 14, but for 25°S, wind stress from 170°E to 90°W, and depth anomalies of the 26.6 sigma isopycnal surface (m) from 170°E to 100°W.

using the same longwave approximation, the phase speed of a mode-1 Rossby wave is 2–3 cm s^{-1}, and the time for these waves to cross the Pacific is roughly 15–21 yr. Positive wind stress and positive depth anomalies, along with positive IPO and negative STC, can be seen around years 625, 645, 685, 760, 790, 835, and 870. Negative wind stress initiating negative depth anomalies in association with negative IPO and positive STC is seen near years 615, 635, 670, 720, and 850.

The transit time for these off-equatorial Rossby waves in the model in each hemisphere is between about 14–20 yr, which sets the multidecadal time scale. A similar contribution to multidecadal variability in the Pacific was noted in the model analysis of Knutson and Manabe (1998).

Figure 16 shows the connection between the Rossby waves at 25°S (right) and depth anomalies of the 25.85 sigma surface at the equator (with longitudes reversed

at the left to run from west to east). This is similar to what also happens at 20°N (not shown). The depth at the equator is chosen since this is near the maximum magnitude of the STCs in Fig. 12 and more indicative of equatorial thermocline depth. The longitude range in Fig. 16 is set up to facilitate following the Rossby waves across 25°S from right to left, and from west to east at the equator at left. Following the Rossby waves from 25°S to the west, once the depth signals reach the equator their propagation to the east is very rapid, on the order of months, or the time scale of equatorial Kelvin waves. Thus, the equatorial depth anomaly signals almost appear flat in Fig. 16.

The connection from 25°S (and 20°N) to the equator is via wave reflection at the western boundary, which can be illustrated for a case that starts at about year 750 with positive depth anomalies and positive IPO in Fig. 16. At 25°S there is a positive wind stress anomaly, and
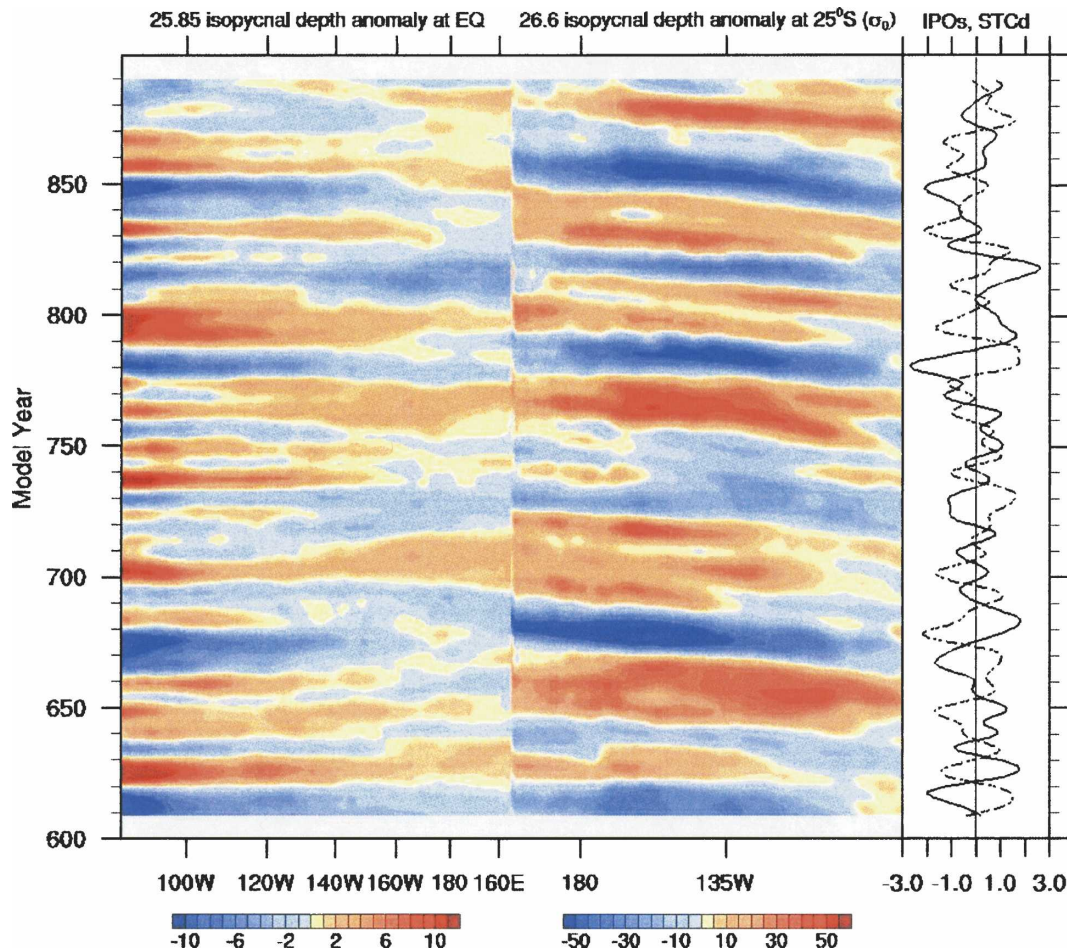
FIG. 16. (right) Same as in Fig. 15, (middle) the same 26.6 sigma depth anomalies at 25°S as the left part of Fig. 15, and (left) the 25.85 sigma depth anomalies at the equator but with longitude values reversed such that the longitude values run, right to left, from 160°E to 80°W. Thus, an anomaly can be traced from right to left as the 26.6 sigma depth anomalies propagating from east to west, then traversing the equatorial Pacific from west to east.

a positive depth anomaly that begins to move west (Fig. 15) is initiated. This positive depth anomaly is shown in Fig. 17a to be approaching the western boundary at the same time a positive depth anomaly at 20°N is reaching the Philippines (highlighted by dark arrows in Fig. 17a). Meanwhile negative depth anomalies from the previous cycle are reflecting to the equator, shallowing the thermocline and producing negative depth anomalies there after year 752 in Fig. 16. The subsequent reflection of the positive depth anomalies can be seen in Fig. 17b as positive depth anomalies extending along the western boundary south from the Philippines and north from the east coast of Australia (highlighted by dark arrows). At the same time the negative depth anomalies that had formed previously are transitioning to positive along the equator as a consequence of the downwelling equatorial Kelvin waves. These waves then reflect at the

eastern boundary to contribute to the ocean Rossby waves near 20°N and 25°S.

To illustrate these wave reflections and connections from 20°N to the equator, lag correlations are calculated between the isopycnal depth anomaly averaged across the equatorial Pacific and isopycnal depth anomalies for three longitude sections at 20°N, one for the western Pacific (115°–150°E; Fig. 17c), one for the mid-Pacific (150°E–125°W; Fig. 17d), and one for the eastern Pacific (125°–105°W; Fig. 17e) for the same time period as in Fig. 16. For the western Pacific, there are small-amplitude negative correlations at zero lag (Fig. 17c) indicating that just before a transition in the equatorial band, there are opposite-sign depth anomalies at 20°N as indicated in Fig. 17a. The small amplitude is due to the difficulties of relating simple longitude segment averages at 20°N as they reflect to the
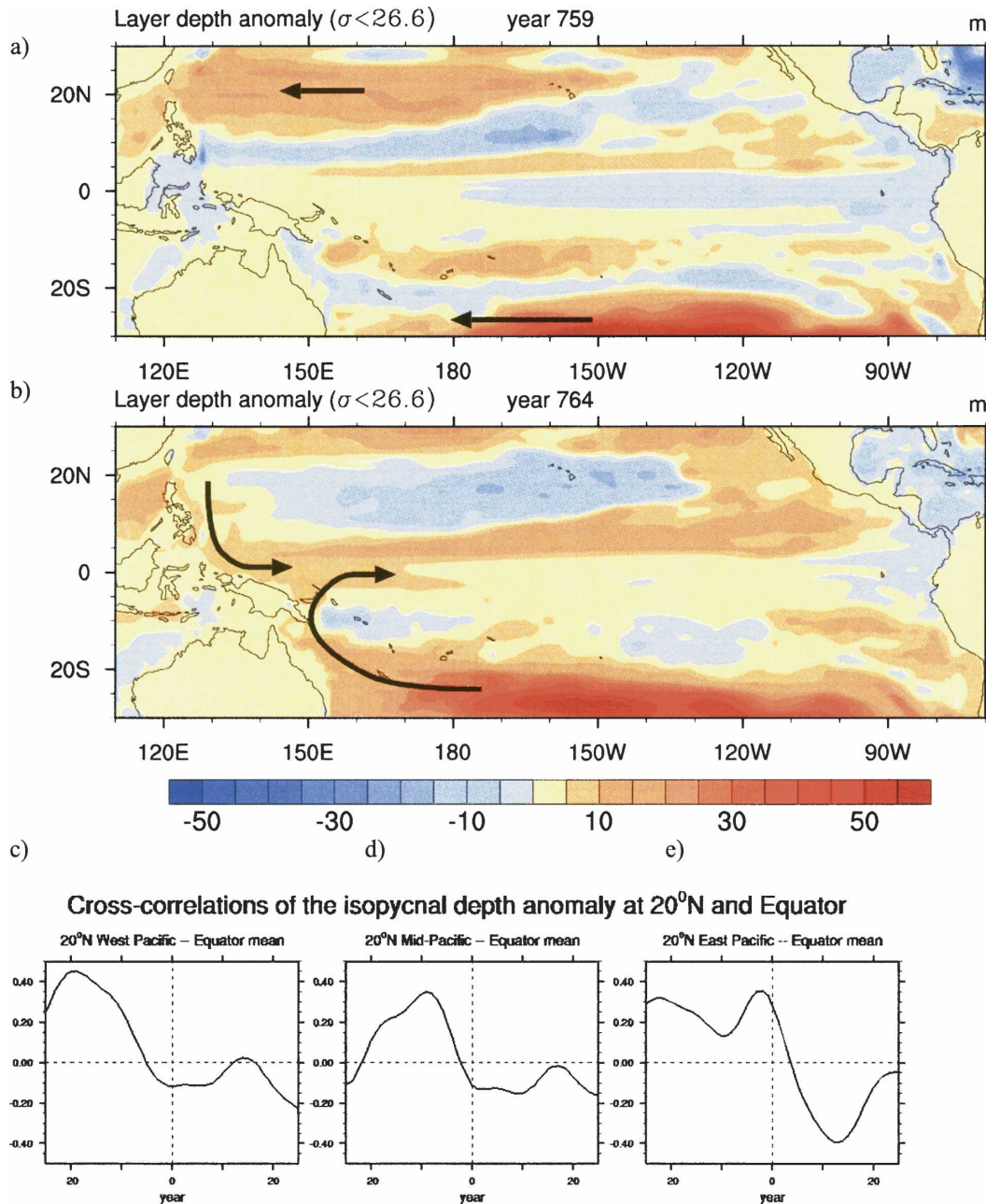
FIG. 17. (a) The 26.6 sigma depth anomalies for year 759 with dark arrows highlighting positive depth anomalies propagating from east to west across the Pacific; note negative depth anomalies in the equatorial Pacific at this time. (b) Same as in (a), but for year 764; note that the positive depth anomalies in (a) have reached the western boundary and indications of reflection toward the equator are given by the positive values right near the western boundary near the Philippines, Papua New Guinea, and Australia and are highlighted by dark arrows; note also that as this is happening, the depth anomalies in the equatorial Pacific are transitioning from negative in (a) to positive in (b). Lag correlations between isopycnal depth anomalies at 20°N in the (c) west Pacific segment (115°–150°E), (d) mid-Pacific segment (150°–125°W), and (e) east Pacific segment (125°–105°W) and the average trans-Pacific isopycnal depth anomalies, such that the equator leads 20°N to the left of the zero lag line, and the equator lags 20°N to the right of the zero lag line.
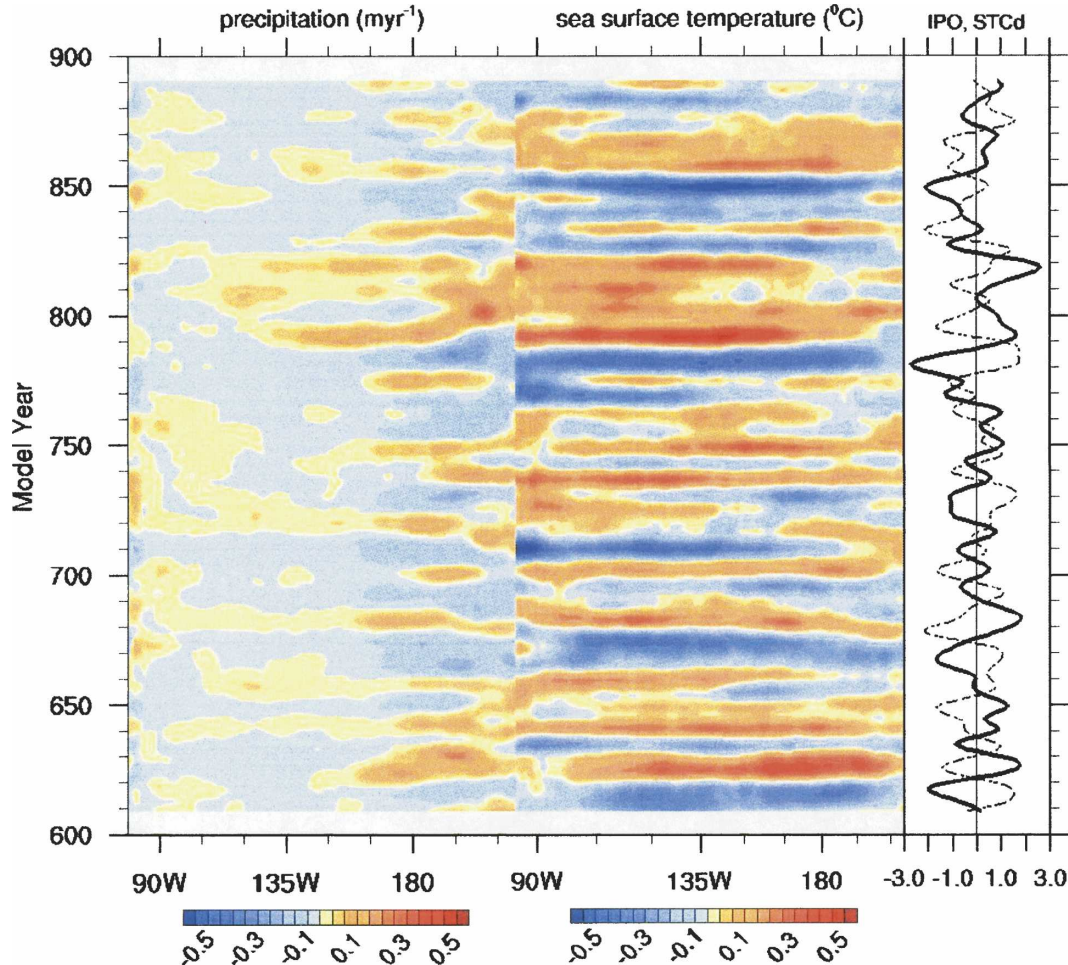
FIG. 18. Same as Fig. 16, but for equatorial SST anomalies at right, running from right to left with longitude values reversed to be consistent with the left side of Fig. 16, ranging from 100°E to 80°W, and precipitation anomalies (averaged from 5°N to 5°S) from 140°E to 70°W also with longitude values reversed.

equator because of the complicated geography of the western boundary as noted above. As the Rossby waves reflect and affect the equatorial depth anomalies, the sign of the lag correlations changes (to the left of the year-0 line in Fig. 17c) as the transition occurs in the equatorial band (Fig. 17b). Then a positive phase of the IPO develops, with positive lag correlations a few years after the transition in the eastern Pacific at 20°N (positive values at about lag −3 in Fig. 17e). This is indicative of the reflection of the equatorial Kelvin waves from the eastern boundary acting in conjunction with the wind forcing from the atmospheric teleconnections to produce like-sign depth anomalies in the eastern Pacific equator and 20°N bands (Fig. 10a). This depth anomaly at 20°N then propagates across the Pacific, producing a positive lag correlation in the mid-Pacific (Fig. 17d) at a lag of 10 yr, and eventually this positive depth anomaly reaches the western Pacific, producing a

positive correlation at a lag of 20 yr in Fig. 17c, where it then reflects to the equator again, starting another cycle. The large negative lag correlations in the eastern Pacific (Fig. 17e) at about lag +13 are indicative of the opposition of the equatorial band and the eastern Pacific at 20°N after the depth anomalies propagate to the west at 20°N and before there is reflection of equatorial anomalies at the eastern boundary.

To highlight these connections in the equatorial Pacific, there are positive depth anomalies at the equator at year 764, SSTs rise, and there is a positive phase of the IPO at far right and positive precipitation anomalies (Fig. 18). Note that Fig. 18 has longitudes reversed for equatorial SST and precipitation to run from east to west (left to right) consistent with the equatorial depth anomalies in Fig. 16. As the trade winds weaken in response to the warming tropical Pacific SSTs, the STCs spin down, providing a positive feedback to deep-

ening the thermocline and contributing to even warmer SSTs. Then, as shown in Fig. 11a, through atmospheric Rossby wave propagation from the positive convective heating anomalies associated with these positive precipitation anomalies, the Aleutian and South Pacific lows deepen (e.g., Deser et al. 2004), and the cycle starts again.

As noted above, the multidecadal time scale is provided by the transit time of the ocean Rossby waves near 20°N and 25°S (roughly 14–20 yr). Thus, when the positive SST anomalies in the tropical Pacific are generating positive wind stress anomalies near 20°N and 25°S, the negative depth anomalies from the previous half-cycle, when the Aleutian and South Pacific lows were shallow in association with the cool phase of the IPO, reach the western boundary, reflect, and propagate across the Pacific to end the warm phase in the equatorial Pacific by shallowing the thermocline and cooling the equatorial Pacific SSTs. These waves reflect, in turn, at the eastern boundary and then contribute to the ocean Rossby waves near 20°N and 25°S. Other studies have also shown how ocean Rossby waves outside the equatorial Tropics (e.g., Capotondi et al. 2003) are tied to equatorial Pacific SSTs (Galanti and Tziperman 2003).

Here the transit time of ocean Rossby waves near 20°N and 25°S is shown to set the decadal time scale and influence subsequent equatorial thermocline depth and SST anomalies. Therefore, a megadrought is most likely to occur when the wind forcings in both hemispheres are synchronized and long lasting. The atmospheric Rossby wave response from convective heating anomalies in the tropical Pacific on the decadal time scale does tend to be synchronous in each hemisphere (e.g., with the North and South Pacific troughs reacting in the same sense; see Seager et al. 2003 and Figs. 11 and 13).

6. Conclusions

A global coupled climate model is analyzed to study the processes involved with producing megadroughts over the southwestern United States and Indian monsoon regions. We formulate a definition for a megadrought based on a threshold duration criterion and note that such events are somewhat longer-lived extremes in inherent multidecadal precipitation variability over these regions. This precipitation variability is closely tied to a multidecadal pattern of SST anomalies in the Pacific Ocean. Thus, to understand the multidecadal precipitation variability that results in megadroughts, we must diagnose the mechanism that is producing the multidecadal SST variability in the Pacific.

We find that the mechanism involves a combination of coupled tropical–midlatitude, air–sea processes where the multidecadal time scale is set by the transit time of wind-forced ocean Rossby waves near 20°N and 25°S near the poleward limits of the STCs. We can summarize this mechanism as follows (depicted schematically in Fig. 19):

- The IPO positive phase is characterized by a warm tropical Pacific, weak trade winds and STCs, positive precipitation and convective heating anomalies, and extended Indian monsoon region drought with the Great Basin anomalously wet. The atmospheric Rossby wave response intensifies the Aleutian and South Pacific lows and westerly surface wind stress anomalies extend to off-equatorial Tropics (e.g., ~20°N and 25°S; Fig. 19a).
- The wind forcing, supplemented by wave reflections from the equatorial eastern Pacific, produces positive ocean layer thickness anomalies at those latitudes that begin to propagate westward as downwelling Rossby waves (Fig. 19a).
- Negative layer thickness anomalies from the previous cold tropical Pacific period arrive at the western boundary and propagate to the equatorial Tropics acting to shallow the thermocline via upwelling Kelvin waves.
- East Pacific SSTs cool and the trade winds strengthen, spinning up the STCs, which results in shallowing of the thermocline and SSTs cool even more. The Great Basin experiences extended dry conditions and the Indian monsoon becomes anomalously strong (Fig. 19b).
- The atmospheric Rossby wave response weakens the Aleutian and South Pacific lows, and easterly wind stress anomalies extend to the off-equatorial Tropics (e.g., ~20°N and 25°S; Fig. 19b).
- Negative layer thickness anomalies form and begin to propagate westward as upwelling Rossby waves (Fig. 19b).
- The period of extended strong monsoon conditions begins to subside and the Pacific trade winds weaken. Positive layer thickness anomalies from the previous warm tropical Pacific arrive at the western boundary and propagate to the equatorial Tropics to deepen the thermocline via downwelling Kelvin waves.
- The eastern Pacific SSTs warm, the trade winds weaken, STCs spin down, and the SSTs warm even more. The extended Indian monsoon region has dry conditions with Great Basin anomalously wet (Fig. 19a), and so on, to begin the cycle again.

Once the tropical Pacific SST anomalies are established on the multidecadal time scale, the precipitation
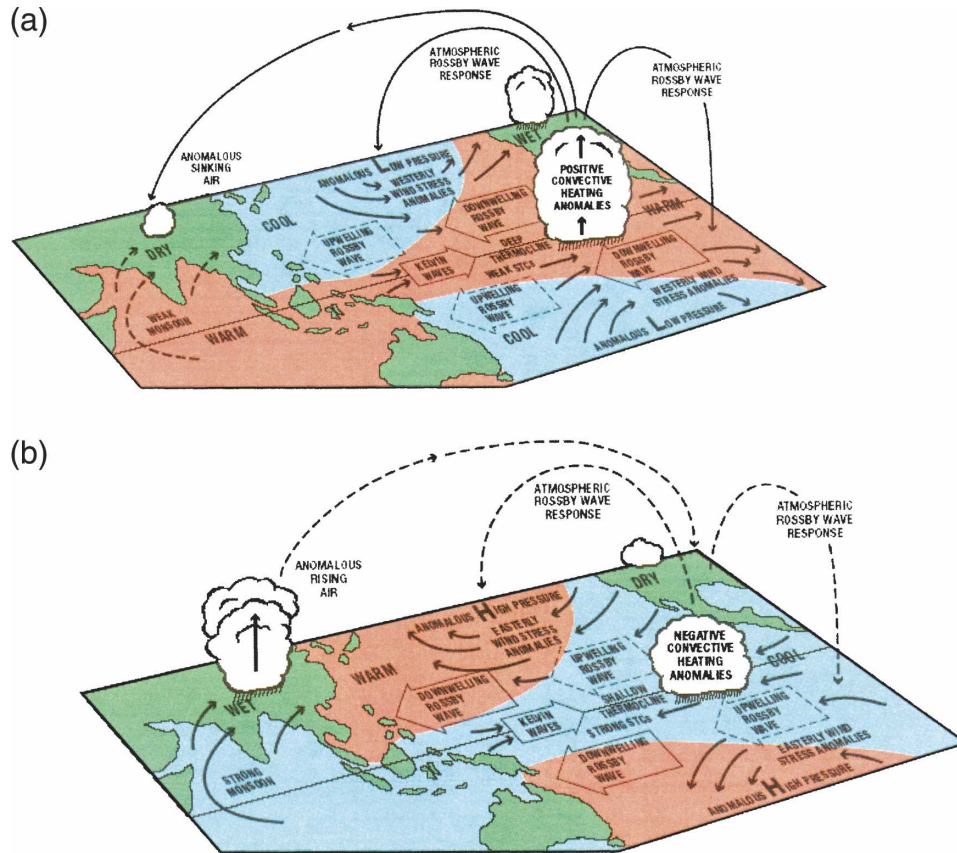
(a)

(b)

FIG. 19. Schematic diagram of the coupled atmosphere–ocean tropical–midlatitude mechanism that produces multidecadal precipitation variability over the Great Basin region in the southwestern United States and the Indian monsoon region with extremes in the multidecadal oscillation being manifested as megadroughts in those regions. (a) The phase when the IPO is positive with multidecadal drought in the Indian monsoon region and anomalously wet conditions in the Great Basin region in the southwestern United States, with relatively warm SSTs and positive convective precipitation and convective heating anomalies in the tropical Pacific, deeper low pressure centers in the midlatitude North Pacific and South Pacific, and anomalous westerly wind stress anomalies extending down to 20°N and 25°S forcing down-welling ocean Rossby waves that begin to travel westward. Farther west are upwelling ocean Rossby waves forced by easterly wind stress anomalies 10–15 yr earlier reaching the western boundary where they will make their way to the equatorial Pacific and be manifested as eastward-propagating upwelling ocean Kelvin waves that act to shallow the thermocline. Equatorial Pacific SSTs cool, and trade winds strengthen, spinning up the STCs, which further act to shallow the thermocline and contribute to even cooler tropical Pacific SSTs. This leads to (b) the phase when the IPO is negative with multidecadal wet conditions in the Indian monsoon region and drought conditions in the Great Basin region in the southwestern United States, with relatively cool SSTs and negative precipitation and convective heating anomalies in the tropical Pacific, shallower low pressure centers in the midlatitude North and South Pacific, and anomalous easterly wind stress anomalies extending down to 20°N and 25°S forcing up-welling ocean Rossby waves that begin to travel westward. Farther west are the downwelling ocean Rossby waves that were forced by the westerly wind stress anomalies 10–15 yr earlier at top reaching the western boundary where they will make their way to the equatorial Pacific and be manifested as eastward-propagating downwelling ocean Kelvin waves that act to deepen the thermocline. Equatorial Pacific SSTs warm, and trade winds weaken, spinning down the STCs, which further act to deepen the thermocline and contribute to even warmer tropical Pacific SSTs that return the system to the state in (a).

anomalies associated with megadroughts in the Great Basin and Indian monsoon regions react as noted in Fig. 11a. Thus, we have shown that an understanding of the mechanism that produces multidecadal SST anoma-

lies in the tropical Pacific is critical to explaining mega-droughts in the Great Basin and Indian monsoon regions.

The analyses here demonstrate that multidecadal precipitation variability over south Asia and the south-

western United States is necessarily irregular, spanning a range of time scales from about 15 to 30 yr. Megadroughts, as defined here, are the extremes of this multidecadal variability and occur roughly every century and a half in the model. This broad time-scale range is due to the myriad of factors that must combine to produce such extended precipitation anomalies, a number of which we have identified from the model analyses in this paper. Though the midlatitude atmospheric circulation responds similarly in each hemisphere to the tropical convective heating anomalies on this time scale, the transit distance of the wind-forced ocean Rossby waves near 20°N and 25°S is not the same in each hemisphere because of the different geometry of the North Pacific and South Pacific basins. For example, depending on the longitude and hemisphere in which they originate, different crossing times can then transpire, producing a range of time scales. For a megadrought to occur, as noted above, ideally there are contributions to Pacific thermocline depth anomalies from each hemisphere to produce as large a multidecadal signal in the equatorial Pacific as possible, with feedbacks from coupled interactions in the tropical Pacific between thermocline depth, SST, wind stress, and STC strength. Clearly many of these factors can combine together in different ways to produce mild droughts, extended megadroughts, or a weak multidecadal signal.

Results presented in this paper show plausible consistency relationships among various interacting coupled processes. A more definitive demonstration of these mechanisms would require sensitivity experiments formulated with the coupled model or a version of a stand-alone ocean model. Though beyond the scope of the present paper, we are presently exploring the feasibility of such experiments.

Since there are so many interacting processes taking place over such a large part of the Indo-Pacific region with varying but multidecadal time scales, it is evident that each multidecadal event has its own combination of processes, with many of these processes classified as necessary but not sufficient, but taken together they can produce a megadrought. This is not unlike the individual nature of El Niño events, or interannual monsoon droughts, with such events having mechanisms in common, but with a number of possible processes contributing to the manifestation of each event. We have shown here that multidecadal phenomena, such as megadroughts, have a similar character, with some processes acting in common to produce them, but with a variety of contributing interactions that can influence the exact period, duration, or amplitude of each event. Thus, this signal-to-noise problem will make it difficult, as with ENSO, to determine if changes in external forc-

ing from, for example, anthropogenic greenhouse gases, will alter the characteristics of megadroughts in the future.

REFERENCES

Acuna-Soto, R., D. W. Stahle, M. K. Cleaveland, and M. D. Therrell, 2002: Megadrought and megadeath in 16th century Mexico. *Emerging Infect. Dis.,* **8,** 360–362.

Alexander, M. A., I. Blade, M. Newman, J. R. Lanzante, N.-C. Lau, and J. D. Scott, 2002: The atmospheric bridge: The influence of ENSO teleconnections on air–sea interaction over the global oceans. *J. Climate,* **15,** 2205–2231.

Ammann, C. M., G. A. Meehl, W. M. Washington, and C. Zender, 2003: A monthly and latitudinally varying volcanic forcing dataset in simulations of 20th century climate. *Geophys. Res. Lett.,* **30,** 1657, doi:10.1029/2003GL016875.

Arblaster, J. M., G. A. Meehl, and A. Moore, 2002: Interdecadal modulation of Australian rainfall. *Climate Dyn.,* **18,** 519–531.

Barlow, M., H. Cullen, and L. Bradfield, 2002: Drought in central and southwest Asia: La Nina, the warm pool, and Indian Ocean precipitation. *J. Climate,* **15,** 697–700.

Bonan, G. B., 1996: A land surface model (LSM version 1) for ecological, hydrological, and atmospheric studies: Technical description and user's guide. NCAR Tech. Note NCAR TN-417+STR, National Center for Atmospheric Research, Boulder, CO, 150 pp.

Capotondi, A., and M. A. Alexander, 2001: Rossby waves in the tropical Pacific and their role in decadal thermocline variability. *J. Phys. Oceanogr.,* **31,** 3496–3515.

——, ——, and C. Deser, 2003: Why are there Rossy wave maxima in the Pacific at 10°S and 13°N? *J. Phys. Oceanogr.,* **33,** 1549–1563.

Cook, E. R., C. A. Woodhouse, C. M. Eakin, D. M. Meko, and D. W. Stahle, 2004: Long-term aridity changes in the western United States. *Science,* **306,** 1015–1018.

Dai, A., G. A. Meehl, W. M. Washington, and T. M. L. Wigley, 2001a: Ensemble simulations of twenty-first century climate changes: Business-as-usual versus CO$_2$ stabilization. *Bull. Amer. Meteor. Soc.,* **82,** 2377–2388.

——, T. M. L. Wigley, G. A. Meehl, and W. M. Washington, 2001b: Effects of stabilizing atmospheric CO$_2$ on global climate in the next two centuries. *Geophys. Res. Lett.,* **28,** 4511–4514.

Deser, C., A. S. Phillips, and J. W. Hurrell, 2004: Pacific interdecadal variability: Linkages between the Tropics and the North Pacific during boreal winter since 1900. *J. Climate,* **17,** 3109–3124.

Galanti, E., and E. Tziperman, 2003: A midlatitude ENSO tele-connection mechanism via baroclinically unstable long Rossby waves. *J. Phys. Oceanogr., 33,* 1877–1888.

Gill, A. E., 1982: *Atmosphere-Ocean Dynamics.* Academic Press, 662 pp.

Glantz, M., 1987: *Drought and Hunger in Africa.* Cambridge University Press, 457 pp.

——, 1994: *Drought Follows the Plow: Cultivating Marginal Areas.* Cambridge University Press, 197 pp.

Gu, D., and S. G. H. Philander, 1997: Interdecadal climate fluctuations that depend on exchange between the tropics and extratropics. *Science, 275,* 805–880.

Hoerling, M., and A. Kumar, 2003: The perfect ocean for drought. *Science, 299,* 691–694.

Jin, F.-F., 1997: A theory of interdecadal climate variability of the North Pacific ocean–atmosphere system. *J. Climate, 10,* 1821–1835.

Kleeman, R., J. P. McCreary, and B. A. Klinger, 1999: A mechanism for the decadal variation of ENSO. *Geophys. Res. Lett., 26,* 1743–1747.

Knutson, T. R., and S. Manabe, 1998: Model assessment of decadal variability and trends in the tropical Pacific Ocean. *J. Climate, 11,* 2273–2296.

Krishnan, R., and M. Sugi, 2003: Pacific decadal oscillation and variability of the Indian summer monsoon rainfall. *Climate Dyn., 21,* 233–242.

Latif, J., and T. P. Barnett, 1994: Causes of decadal climate variability over the North Pacific and North America. *Science, 266,* 634–637.

Lee, T., and I. Fukumori, 2003: Interannual-to-decadal variations of tropical–subtropical exchange in the Pacific Ocean: Boundary versus interior pycnocline transports. *J. Climate, 16,* 4022–4042.

Leith, C. E., 1973: The standard error of time-average estimates of climatic means. *J. Appl. Meteor., 12,* 1066–1069.

Liu, Z., and H. Yang, 2003: Extratropical control of tropical climate, atmosphere bridge and ocean bridge. *Geophys. Res. Lett., 30,* 1230, doi:10.1029/2002GL016492.

——, L. Wu, R. Gallimore, and R. Jacob, 2002: Search for the origins of Pacific decadal climate variability. *Geophys. Res. Lett., 29,* 1404, doi:10.1029/2001GL013735.

Loschnigg, J., G. A. Meehl, P. J. Webster, J. M. Arblaster, and G. P. Compo, 2003: The Asian monsoon, the tropospheric biennial oscillation, and the Indian Ocean Dipole in the NCAR CSM. *J. Climate, 16,* 2138–2158.

Mantua, N. J., S. R. Hare, Y. Zhang, J. M. Wallace, and R. C. Francis, 1997: A Pacific interdecadal oscillation with impacts on salmon production. *Bull. Amer. Meteor. Soc., 78,* 1069–1079.

McPhaden, M. J., and D. Zhang, 2002: Slowdown of the meridional overturning circulation in the upper Pacific Ocean. *Nature, 415,* 603–608.

Meehl, G. A., 1987: The annual cycle and interannual variability in the tropical Pacific and Indian Ocean regions. *Mon. Wea. Rev., 115,* 27–50.

——, 1997: The south Asian monsoon and the tropospheric biennial oscillation. *J. Climate, 10,* 1921–1943.

——, and J. Arblaster, 1998: The Asian–Australian monsoon and El Niño–Southern Oscillation in the NCAR Climate System Model. *J. Climate, 11,* 1357–1387.

——, and ——, 2002: The tropospheric biennial oscillation and Asian–Australian monsoon rainfall. *J. Climate, 15,* 722–744.

——, ——, and W. G. Strand, 1998: Global scale decadal climate variability. *Geophys. Res. Lett., 25,* 3983–3986.

——, P. Gent, J. M. Arblaster, B. Otto-Bliesner, E. Brady, and A. Craig, 2001: Factors that affect amplitude of El Niño in global coupled climate models. *Climate Dyn., 17,* 515–526.

——, W. M. Washington, T. M. L. Wigley, J. M. Arblaster, and A. Dai, 2003: Solar and greenhouse gas forcing and climate response in the twentieth century. *J. Climate, 16,* 426–444.

——, ——, C. Ammann, J. M. Arblaster, T. M. L. Wigley, and C. Tebaldi, 2004a: Combinations of natural and anthropogenic forcings and twentieth-century climate. *J. Climate, 17,* 3721–3727.

——, ——, J. M. Arblaster, and A. Hu, 2004b: Factors affecting climate sensitivity in global coupled models. *J. Climate, 17,* 1584–1596.

——, ——, W. D. Collins, J. M. Arblaster, A. Hu, L. E. Buja, W. G. Strand, and H. Teng, 2005: How much more global warming and sea level rise? *Science, 307,* 1769–1772.

Miller, A. J., and N. Schneider, 2000: Interdecadal climate regime dynamics in the North Pacific Ocean: Theories, observation and ecosystem impacts. *Progress in Oceanography,* Vol. 27, Pergamon, 257–260.

New, M., M. Todd, M. Hulme, and P. Jones, 2001: Precipitation measurements and trends in the twentieth century. *Int. J. Climatol., 21,* 1899–1922.

Nonaka, M., S.-P. Xie, and J. P. McCreary, 2002: Decadal variations in the subtropical cells and equatorial Pacific SST. *Geophys. Res. Lett., 29,* 1116, doi:10.1029/2001GL013717.

Pierce, D. W., T. P. Barnett, and M. Latif, 2000: Connections between the Pacific Ocean Tropics and midlatitudes on decadal timescales. *J. Climate, 13,* 1173–1194.

Power, S., T. Casey, C. Folland, A. Colman, and V. Mehta, 1999: Interdecadal modulation of the impact of ENSO on Australia. *Climate Dyn., 15,* 319–324.

Rasmusson, E. M., and T. H. Carpenter, 1983: The relationship between eastern equatorial Pacific sea surface temperatures and rainfall over India and Sri Lanka. *Mon. Wea. Rev., 111,* 517–528.

Rayner, N., D. Parker, E. Horton, C. Folland, L. Alexander, D. Rowell, E. Kent, and A. Kaplan, 2003: Global analyses of sea surface temperature, sea ice, and night marine air temperature since the late nineteenth century. *J. Geophys. Res., 108,* 4407, doi:10.1029/2002JD002670.

Schneider, N., A. J. Miller, and D. W. Pierce, 2002: Anatomy of North Pacific decadal variability. *J. Climate, 15,* 586–605.

Schubert, S. D., M. J. Suarez, P. J. Pegion, R. D. Koster, and J. T. Bacmeister, 2004: On the cause of the 1930s Dust Bowl. *Science, 303,* 1855–1859.

Seager, R., N. Harnik, Y. Kushner, W. Robinson, and J. Miller, 2003: Mechanisms of hemispherically symmetric climate variability. *J. Climate, 16,* 2960–2978.

Solomon, A., J. P. McCreary Jr., R. Kleeman, and B. A. Klinger, 2003: Interannual and decadal variability in an intermediate coupled model of the Pacific region. *J. Climate, 16,* 383–405.

Trenberth, K. E., and G. W. Branstator, 1992: Issues in establishing causes of the 1988 drought over North America. *J. Climate, 5,* 159–172.

Washington, W. M., and Coauthors, 2000: Parallel climate model (PCM) control and transient simulations. *Climate Dyn., 16,* 755–774.

Wu, L., Z. Liu, R. Gallimore, R. Jacob, D. Lee, and Y. Zhong, 2003: Pacific decadal variability: The tropical Pacific mode and the North Pacific mode. *J. Climate, 16,* 1101–1120.

Zhang, Y., J. M. Wallace, and D. S. Battisti, 1997: ENSO-like interdecadal variability: 1900–1993. *J. Climate, 10,* 1004–1020.